Received: 15 July 2023 | Revised: 27 October 2023 | Accepted: 14 November 2023

DOI: 10.1111/jace.19644

Journal of the American Ceramic Society

RESEARCH ARTICLE

Characterizing stress development and cracking of ceramic particulate coatings during drying

Annie Moorhead | **Lorraine F. Francis**

Department of Chemical Engineering and Materials Science, University of Minnesota, Minneapolis, Minnesota, USA

Correspondence
Lorraine F. Francis, Department of Chemical Engineering and Materials Science, University of Minnesota, Minneapolis, MN 55455, USA.
Email: lfrancis@umn.edu

Funding information
MRSEC, Grant/Award Number: DMR-2011401; NNCI, Grant/Award Number: ECCS-2025124; NNCI, Grant/Award Number: ECCS-2025124

Abstract

During drying, liquid-applied particulate coatings develop stress and are consequently prone to stress-induced defects, such as cracking, curling, and delamination. In this work, the stress development and cracking of coatings, prepared from aqueous silica and zinc oxide particle suspensions, were characterized using cantilever beam deflection with simultaneous imaging of the coating surface. Drying uniformity was improved and lateral or edge-in drying was discouraged by using thin silicone walls around the perimeter of the cantilever. Coatings prepared from larger monodisperse silica particles (D_{50} ~ 0.9 μm) dried uniformly but had a high critical cracking thickness (>150 μm) that prevented simultaneous study of stress development and cracking. Coatings prepared from smaller silica particles (D_{50} ~ 0.3 μm) cracked readily at low thicknesses but exhibited edge-in drying that complicated the stress measurement data. This drying nonuniformity was connected to the potential for these small particles to accumulate at the coating surface during drying. Hence, the selection of particle size and density was critical to drying uniformity when characterizing stress development and cracking. Coatings prepared from suspensions of zinc oxide particles (D_{50} ~ 0.4 μm) were well-suited for these studies, with uniform drying stress peaking at ~1 MPa. Characteristic features in the stress development data above and below the critical cracking thickness (53 μm) were identified, demonstrating that cantilever beam deflection is a useful tool for studying the effectiveness of crack mitigation methods and the fundamentals of coating fracture during drying.

KEYWORDS
coatings, cracks/cracking, drying, stress

1 | INTRODUCTION

Particulate coatings have a variety of applications, including anticorrosive coatings,[1] battery electrodes,[2] and conductive inks.[3] For optimum properties and performance, uniform coatings that are free of defects, such as delamination and cracks, are required. Fracture mitigation is especially desirable for the production of fuel cells,[4]

battery electrodes,[5] printed electronics,[6] and inverse opals.[7] Therefore, stress development and cracking in particle-based coatings, especially those prepared from ceramic suspensions, has been studied for many years.[8–12]

The understanding of how stress develops during drying has been advanced by experimental studies that employed various stress measurement techniques[9,10,13,14] and coating systems.[10,12] In foundational work, Chiu and Cima[9] measured the stress development during the drying of alumina coatings prepared from aqueous suspensions. They found that coatings were supersaturated with water and largely stress-free in the early stages of drying, followed by an increase in stress to a peak and a stress decrease until the coating was fully dry. In their findings, the peak stress was proportional to the liquid surface tension (γ) and inversely proportional to the particle radius. Hence, they proposed that stress in the coating is related to the capillary pressure, ($\Delta P \propto \frac{\gamma}{R}$) that forms due to the presence of liquid menisci in the pores of a drying particle network, given that the meniscus radius (R) scales with particle size.

Price et al.[11] confirmed the role of capillary pressure by using cryogenic scanning electron microscopy (Cryo-SEM) to image frozen microstructures of aqueous ceramic coatings at various stages of drying and stress development. They found that when the coating stress reached a peak, liquid menisci were present between particles at the top surface of the coating. At this point, the lowered pressure in the liquid from the curved menisci attempts to pull the particle network together, but the shrinkage is constrained due to adherence to the substrate, and an in-plane tensile stress results. As the water continued to evaporate, the coating stress decreased as the menisci receded into the porous particulate network, and less of the coating was subjected to the capillary pressure. Eventually, pendular rings formed at the particle-particle contacts, and coatings had a small residual stress. The findings of this work aligned with those of Chiu and Cima.[9]

In addition to introducing the role of capillarity in coating stress, Chiu and Cima noted conditions where gradients in saturation formed over the coating area during the drying of particulate coatings.[9] Bauer et al.[10] observed similar gradients with a transparent substrate deflection method. They sought conditions for uniform drying, which they defined as homogenous saturation over the coating area during drying. Likewise, both studies[9,10] observed situations where a drying front propagated from the edges of the coating inward. In drying droplets of suspensions, consolidation of the particles begins at the droplet edge in what is often called the "coffee ring effect".[15] Edge-in drying results from the coupling of enhanced evaporation at the contact line due to its curvature and convective flow carrying particles from the middle of the droplet toward the pinned contact line. This effect leads to a compaction front that travels laterally from the edge toward the center. The propagation of this front is frequently referred to as lateral drying.[8,11,16] Analytical expressions used in stress measurement,[17] assume homogeneous drying conditions; hence, the effect of lateral and nonuniform drying on the validity of stress measurement is of concern.[10]

Several approaches have been taken to address these concerns. Chiu and Cima[9] observed increased saturation uniformity by decreasing the evaporation rate and the size of their coating area. Price et al. [11] added polydimethylsiloxane walls around the coating area to mitigate the effects of lateral drying during stress measurement. The walls encouraged uniform top-down drying or vertical drying, which improved drying uniformity and the accuracy of cantilever beam-based stress measurement. For example, they found that aqueous alumina coatings prepared on cantilevers with walls experienced a delayed onset of stress development, a steep stress rise, and a higher peak stress as compared with coatings dried on cantilevers without the walls present. Price et al.[11] did not explore stress development in coatings that crack.

In contrast, several authors have taken advantage of lateral[8,16] or directional[18–20] drying to study coating fracture fundamentals independent of stress measurement. Holmes et al.[8] utilized laser speckle interferometry to determine that particulate networks remain saturated during fracture in laterally dried suspensions. Goehring et al.[18] later demonstrated that prior to cracking, two zones of network formation occur with directional drying: an organized packing zone followed by an aggregation zone. They found that particles initially organize at a packing front and then aggregate into a network, where the particles are in contact. They observed that cracks extend into the aggregated network before the pore space empties and the coating is fully dry.

Another method for characterizing coating fracture resistance is to find the critical cracking thickness (CCT).[21,22] Coatings prepared with a thickness above the CCT crack, while those with a thickness below the CCT remain crack-free during drying. A higher CCT indicates a greater resistance to fracture. Chiu et al.[21] studied the effect of various coating formulations and processing conditions on the CCT experimentally. Additional research has predicted relationships between particle size, coating thickness, and fracture for both soft[23] and hard[24,25] particle systems. Thus, the drying stress both above and below the CCT is of interest.

Previous studies of stress development have been limited to crack-free coatings in part because fracture relieves stress, which impacts the interpretation of stress measurement results.[26] Additionally, some investigations of stress development in hard particle cracking coatings have observed gradients in saturation consistent with lateral drying,[8] which complicates interpretation. Thus, the characterization of stress development and cracking in the

TABLE 1 Particle size from laser diffraction and suspension information.

Name	D_{10} (μm)	D_{50} (μm)	D_{90} (μm)	Span*	Particle loading
Silica-M0.9	0.747	0.873	0.959	0.242	30 vol%
Silica-M0.3	0.246	0.272	0.338	0.338	30 vol%
ZnO-P0.4	0.224	0.435	0.971	1.72	20 vol%

*Span is defined as $(D_{90}-D_{10})/D_{50}$; lower span indicates a narrower particle size distribution.

absence of lateral drying has yet to be documented. The present work explores the conditions to encourage uniform drying for coatings prepared with walls and presents a model zinc oxide system that exhibits uniform drying as well as cracking. Using this system, the relationship between coating stress and fracture is characterized.

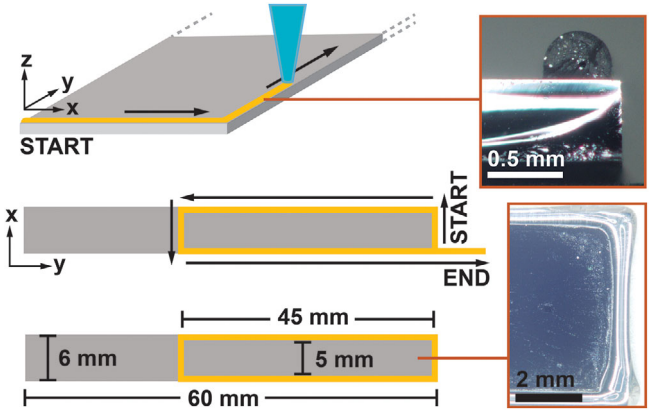

FIGURE 1 Direct ink write printing of walls on silicon substrates. Top: Isometric view of the printing process with digital optical micrograph of the wall cross-section. Middle: The nozzle path for minimizing wall irregularities. Bottom: The final wall geometry with a top-down digital optical micrograph of wall corners. The end of the substrate without walls was later clamped to form a cantilever.

2 | EXPERIMENTAL METHODS

2.1 | Materials

Aqueous suspensions containing silica were prepared as follows. Two sizes of monodisperse silica particles, $D_{50} = 0.272$ μm and $D_{50} = 0.873$ μm, (Itochu Plastics) were studied (Table 1). Suspensions were electrostatically stabilized in water by adjusting the suspension pH. First, a solution of ammonium hydroxide in water was prepared by adding 0.1 M ammonium hydroxide to distilled water until the solution reached a pH of 9. Silica particles were then added to the pH-adjusted solution to give the desired volume percent loading in the suspension. The suspension was stirred for 5 min and then sonicated for 5 min in a bath sonicator (100 W, 42 KHz). This stirring and sonication routine was performed three times so that the particles were adequately dispersed.

Analogously, aqueous zinc oxide suspensions were prepared from a polydisperse zinc oxide powder, D_{50} = 0.435 μm, (US Research Nanomaterials). An aqueous solution containing Darvan C-N dispersant (Vanderbilt Minerals LLC) was prepared, such that the desired dispersant dosage would be 0.35 wt% of the solids in the particle suspension. This dosage is in line with other stability investigations[27] and the manufacturer recommended 0.2–1 wt% based on dry body weight. Particles were then added to the dilute Darvan C-N solution and mixed in the same manner as the silica suspensions. The final suspension had a pH of ~9. The zeta potential (Stabino, Microtrac) of the suspended particles was −41.7 ± 5.36 mV, confirming the suspension stability.

Laser diffraction (Bluewave, Microtrac) was used to characterize the particle size distribution of each suspension formulation. A small volume of each suspension was extracted and then diluted for measurement. Characteristics of the particle size distributions and suspension formulations are summarized in Table 1. Each suspension is named for the type of particle (silica or ZnO), dispersity (monodisperse—M or polydisperse—P), and the approximate D_{50} in microns. When characterized by dynamic light scattering (NanoFlex, Microtrac), Silica-M0.3 was found to have a polydispersity index of 0.0580.

2.2 | Cantilever wall fabrication

A flexible border or wall, similar to that used by Price et al.,[11] was placed around the perimeter of the silicon cantilever beam used in stress measurement to mitigate the effects of lateral drying. Silicon substrates were cut from single-sided or double-sided polished silicon wafers (WaferPro) into 60.0 by 6.0 mm rectangles. A polished side was used for laser reflection in the measurement; there were no observable effects of the surface polish of the opposing side on the stress measurement. Cantilever walls were then 3D printed onto the substrate in a single layer using a custom direct ink write printer.[28] The printer features a pneumatic pressure system for dispensing commercial silicone caulking (GE Silicone 1, Momentive Performance Materials LLC) with a 0.41 mm diameter polypropylene nozzle (Nordson EFD), using a 5 mm/s print speed, 40 psi pneumatic pressure, and 225 μm layer height. For the geometry in Figure 1, a corresponding G-code was generated in Slic3r software and executed within the printer operating software, Repetier (Hot-World

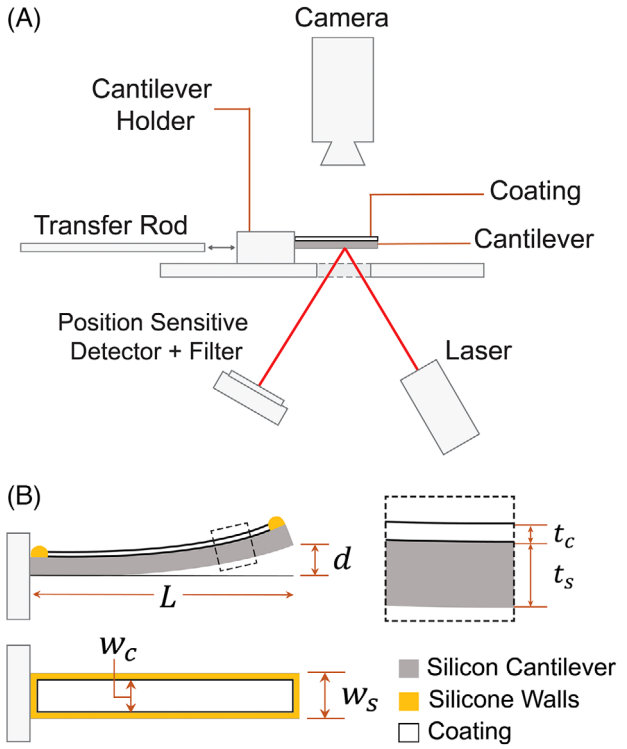

FIGURE 2 (A) Schematic diagram of the components of cantilever beam-based stress measurement apparatus. See text for description. (B) Edge on (mid-plane) and top-down diagrams of the cantilever with geometric parameters in Equations (1) and (2). The deflection is exaggerated and the schematics are not to scale.

GmbH & Co. KG). To confirm the morphology and width of the cantilever walls, images were taken with a digital microscope (Hirox). Images of the final cantilever walls are shown in Figure 1. The final cross-sectional width of the printed walls averaged 450 μm, slightly larger than the print nozzle diameter due to the wetting of the liquid extruded polymer on the substrate.

2.3 | Coating stress measurement

Cantilever beam deflection is a common technique used to quantify the stress developing during drying. The apparatus described in Payne et al.[14] and Price et al.[11] was updated and adapted for this research. Figure 2 shows an overview of the measurement portion of the apparatus, which is mounted on a rigid frame and includes a chamber surrounding the cantilever and appropriate laser safety shielding. A walled silicone substrate was fixed on one end to form a cantilever beam. A diode laser (CVI Melles Griot) was used to generate a beam that reflects off the bottom of the cantilever to a position-sensitive detector (Duma Optronics). A 635 nm bandpass filter (Thorlabs Inc.) was attached to the position-sensitive detector to minimize measurement noise. A digital camera (Hitachi KP-050) and lens assembly (Navitar 1x-6x-0.25x) were used to capture the coating surface during stress measurement. To prepare for an experiment, the substrate is first cleaned and calibrated. The cantilever substrate and its holder are plasma cleaned (Harrick Plasma Inc.) for 1.5 min at 0.9 torr. After cleaning, the cantilever and holder are returned to the apparatus. The cantilever deflection, as measured by the position-sensitive detector, is then calibrated with known displacement from a micrometer pushing on the end of the cantilever.

To prepare for the deposition of the coating, the transfer rod is used to move the cantilever and holder into the coating position, where a small block supports the cantilever. A known volume (34.0-62.8 μL) of suspension is deposited uniformly across the substrate using a micropipette. The deposited suspension levels within ~1–2 seconds of application. The coated cantilever is then pulled into the measurement position, which allows for free deflection. For all measurements, the chamber around the cantilever was open to the air (on the top and on one side) with no additional airflow. Coatings were dried in ambient conditions at temperatures and relative humidities ranging from 22.1–23.4°C and 14%–58% RH. Whenever possible, experiments comparing the effect of suspension deposition volume, or dried coating thickness, were run on the same day to avoid drying rate differences due to RH variation. On any given day, the humidity varied by no more than ±3% RH. When comparing experiments from different days, drying times were normalized to accommodate drying rate differences. The temperature variations were considered negligible. During drying, the cantilever deflected upward due to tensile stress in the coating. The deflection was monitored in situ during drying, and the coating surface was imaged simultaneously using the camera. A Dazzel video capture device and Pinnacle software (Alludo) were used to capture video footage.

The measured deflection (d) was converted into a coating stress (σ) using an analytical expression derived by Corcoran[17]:

$$\sigma = \frac{dE_s {t_s}^3}{3t_c L^2 (t_s + t_c)(1 - \nu_s)} + \frac{dE_c (t_s + t_c)}{L^2 (1 - \nu_c)}, \quad (1)$$

where E_s, t_s, and ν_s are the elastic modulus, thickness, and Poisson's ratio of the substrate, respectively, E_c, t_c, and ν_c are the corresponding values for the coating, and L is the cantilever length. Equation (1) assumes small, one-dimensional deflections and linear elastic mechanics. The second term in Equation (1) is negligible if the thickness and elastic modulus of the coating are much smaller than the corresponding values of the substrate. Using values for the silicon substrate ($t_s = 0.52$ mm and $E_s = 169$ GPa[29]) as well as conservative values for the particulate coatings ($t_c \sim 150$ μm and $E_c \sim 0.2$ GPa[30]), the second term could be

eliminated with <1% error. Hence, this term was not used in the calculation. The decrease in coated area of the substrate associated with the presence of the flexible wall was corrected with a factor determined by the width of the substrate (w_s) relative to the width of the coated area (w_c). This wall has no other mechanical impact on the measurement due to the low modulus of silicone.[11] The resulting expression, Equation (2), was used to convert the measured deflection to coating stress. The elastic modulus and Poisson's ratio of the silicon substrate were taken as 169 GPa and 0.064, respectively.[29]

$$\sigma = \frac{dE_s t_s^3}{3t_c L^2 (t_s + t_c)(1 - \nu_s)} \frac{w_s}{w_c} \tag{2}$$

2.4 | Dried coating thickness characterization

Dried coating thickness was characterized by two methods. First, the average thickness was determined from 30 thickness measurements taken over the coating surface with a digital micrometer (Absolute ID-C112TB, Mitutoyo Corp). Using the average thickness in the conversion of measured deflection to stress is a typical practice.[10,31] In this work, average thicknesses are reported with their respective expanded uncertainties (±Δ) based on a 95% confidence level. Second, an optical microscopy method was used to qualitatively assess cross-sectional thickness uniformity on selected samples. Coated cantilevers were embedded in resin and freeze-fractured to expose the coating cross-section for optical imaging (Hirox). Full details on these characterization methods and resulting data are included in the Supporting Information (S1) available online.

As discussed in the following sections, cantilever walls were effective at preventing premature solidification of the edges and saturation gradients, which is important for understanding the stress development during drying.[10,11] It is important to note, however, that contact line pinning at the walls does lead to an increase in coating thickness adjacent to the walls,[32] as evident in Figure S1 available online. Nevertheless, we expect widthwise thickness gradients to have less impact than lengthwise gradients because they act perpendicular to the one-dimensional deflection. In the present work, the lengthwise thickness variation (≈standard deviation/average thickness) was notably less than the variation over the entire coating area, which includes the widthwise contribution. Due to the uniform saturation and solidification during drying, as well as minimal lengthwise thickness gradients, we believe that calculating stress using an average thickness in Equation (2) is reasonable. Upon propagating the uncertainties from the coating thickness, the expanded uncertainties on the peak stresses reported in this work ranged from 0.1 to 0.2 MPa. More details on this uncertainty analysis are provided in the Supporting Information (S2) available online.

2.5 | Dried coating microstructure imaging

The dried ZnO-P0.4 coating microstructure was characterized using Field Emission Scanning Electron Microscopy, FE-SEM (Hitachi SU8230). To characterize the coating microstructure adjacent to the substrate, double-sided carbon tape was positioned onto a pin mount, then pushed against the top surface of a coating and pulled off to remove pieces of delaminated coating from the substrate. Before imaging, samples were sputter coated (Lecia) with 10 nm of platinum. SEM images were taken at 1.5 kV and 1.0 μA, utilizing the low-angle backscattering detector and the secondary electron detector at 80% suppression.

3 | RESULTS AND DISCUSSION

3.1 | Stress in crack-free and cracking silica particle coatings

Figure 3 shows stress development profiles and representative surface images for coatings prepared from the Silica-M0.9 suspension. Coatings with different thicknesses were prepared by depositing different volumes of suspension (34.0 ± 0.8, 48.8 ± 0.8, and 60.8 ± 0.6 μL) within the walled cantilevers. The average thicknesses of the coatings in Figure 3 were 50 ± 8, 77 ± 10, and 93 ± 16 μm, respectively.

The surface of the drying crack-free coating, as shown in Figure 3 images (A)–(E) using the example of the thickest coating, showed a uniform appearance throughout the coating area, indicating negligible saturation gradients from lateral drying.[11] Thus, the stress development profiles and images in Figure 3 benchmark the case of stress development in crack-free uniformly dried particulate coatings (i.e., those that do not experience an in-plane saturation gradient[10]). The results are consistent with those reported by Price et al.,[11] who used Cryo-SEM to verify the coating microstructure at different stages of drying and stress development for similar monodisperse silica coatings.

The stress profiles in Figure 3 show a delay in the onset of tensile stress development after deposition. The uniform appearance and the absence of stress during this stage indicate that the walls prevent premature solidification of the edges, which would lead to a transient in-plane

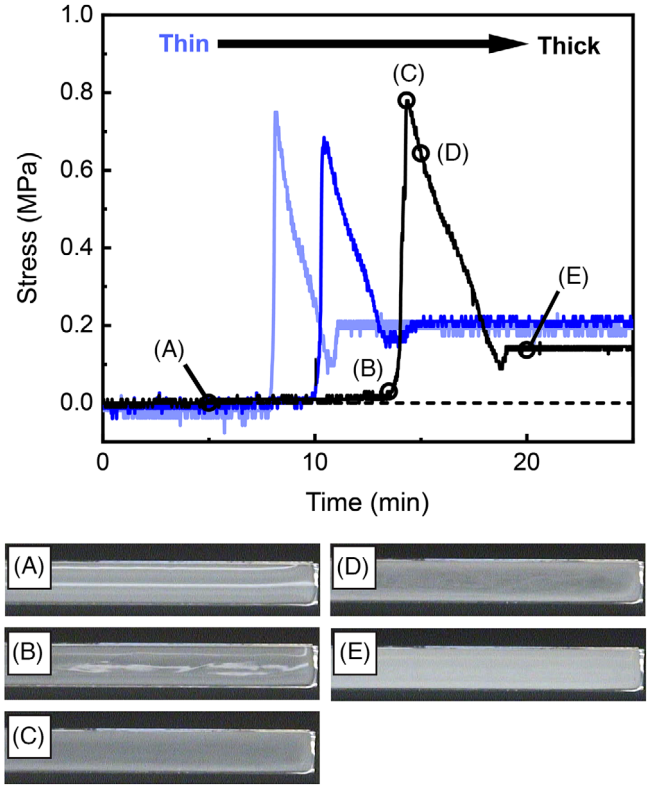

FIGURE 3 Stress development profiles for coatings prepared from Silica-M0.9 suspension. Top: Data for coatings with average thicknesses of 50 ± 8 μm, 77 ± 10 μm and 93 ± 16 μm. Bottom: Images of the surface of the thickest coating taken in situ during drying at time points (A)–(E), as noted on the stress measurement data. Data were collected at 22.6°C and 18% RH.

stress gradient. Based on our in situ images and the work of Price et al.,[11] the suspensions are supersaturated in the early stages of drying. For example, Figure 3 image (A) shows high reflectivity; hence, the coating is still a liquid. Particles rearrange freely as the water evaporates; hence, no stress develops. The surface reflection changes in images (B) and (C) are concurrent with a rapid increase in coating stress. At this stage, the particle concentration is high enough for the formation of a solid particulate network[11] that cannot shrink freely during drying, leading to stress development. The coating appearance becomes translucent, which is especially evident in image (C).

The formation of liquid menisci between particles in the packed network is coincident with the rise in stress to a peak.[11] The magnitude of the stress at this peak depends on the characteristics of the particles, including particle size, as well as the drying conditions. After the stress peak, further drying leads to a decrease in stress as the liquid menisci recede and less of the coating is under the action of the capillary pressure. The formation of air-filled pores leads to an increase in scattering and brightness of the coating; see Figure 3 image (D). Ultimately, the coating reached a final nonzero value for stress (E), likely due to residual water within the network.[11] Prior to reaching this final residual value, there was a dip in stress. This dip has been observed in other stress measurement profiles[9] and may be a result of local particle rearrangement before reaching the residual stress value.

As evident in Figure 3, the stress profiles of coatings from all three coating thicknesses have similar shapes, though thicker coatings experience a longer initial stress-free period. The point of peak stress occurred later for thicker coatings due to the additional water evaporation needed to reach the concentration for a packed particle network. For the range of thicknesses tested, the peak stress showed no dependence on average coating thickness. In prior work, Perera[33] studied the effect of thickness on coatings prepared from suspensions containing pigments and latex binders and also found no detectable change in the maximum stress with thickness.

Unfortunately, the Silica-M0.9 coating system could not be used to study stress development and fracture. The CCT of the coating was over 150 μm. Achieving this high thickness would require much taller walls and would lead to a larger error when neglecting the second term in Equation (1). The Silica-M0.3 suspension, containing smaller silica particles, was therefore selected for analyzing coating stress and fracture. The smaller particle size[21,24] contributed to a lower CCT (<20 μm). Images showing the resulting coating microstructure at the top surfaces of both silica coatings are shown in Figure 4.

Figure 5 shows stress development and images of the coating surface for coatings prepared using Silica-M0.3. Initially, the coating was stress-free and in a supersaturated state, as demonstrated by the reflectance in image (A). Beginning in image (B), a lateral drying front moves inward from the free end of the cantilever. Ahead of the lateral front, the supersaturated suspension reflects light back to the camera. Behind the lateral front, the coating appeared translucent and matte gray in color, indicating a saturated compacted network. Stress begins to rise with the onset of the lateral drying front, demonstrating the connection between local solidification and a gradual stress increase.[11,16]

In Figure 5 image (C), an opaque white color consistent with a dried porous coating appears near the free end. Faint streaks of porous white coating extend from the wall into the center of the translucent compacted network and follow along cracks. Meanwhile, the reflective supersaturated region ahead of the lateral front continues to recede into the coating center. At the time of peak stress, the lateral front dissipates into a local depression or trench[8] as saturation gradients remain. After the peak, stress drops rapidly and then gradually as the remaining water evaporates. When the coating is fully dry, as in image (E), the

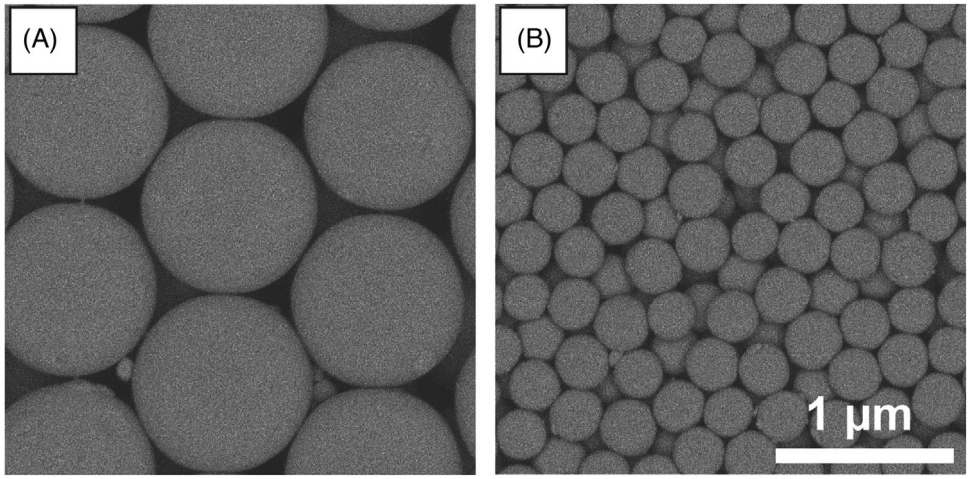

FIGURE 4 SEM images taken at the top surface of coatings made from (A) Silica-M0.9 and (B) Silica-M0.3 suspensions.

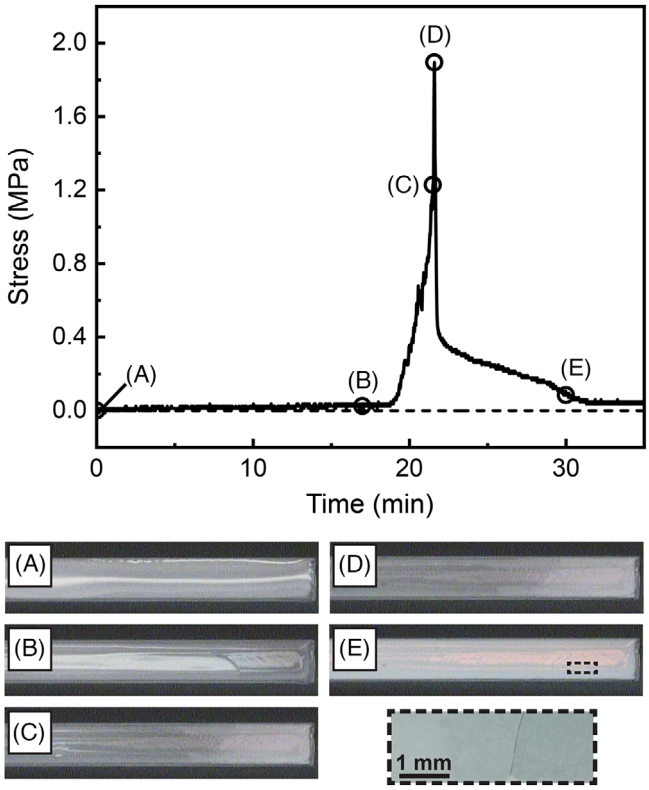

FIGURE 5 Stress development for coatings prepared from Silica-M0.3. Top: Stress measurement data for a coating with an average coating thickness of 77 ± 8 μm. Bottom: Images of the coating surface taken in situ at the time points indicated. The magnified image on the bottom right shows cracking on the dried coating surface (E). Data were collected at 22.1°C and 56% RH.

coating displays opalescence, which indicates organized particle packing at the surface.[34] As demonstrated in the higher magnification image of the final dried coating surface (see Figure 5), the coating cracked during drying. Cracks perpendicular to the coating wall were apparent along the cantilever length. Though the coating cracked as anticipated, the stress measurement results were not ideal because lateral drying occurred despite the presence of the walls.

3.2 | Effect of particle distribution on drying uniformity

Given the nonuniformity in saturation during drying shown in Figure 5, the interpretation of stress development and fracture was not clear. One hypothesis is that the difficulty in uniformly drying the Silica-M0.3 system is linked to particle distribution through the coating thickness during drying, which can be predicted using the model developed by Cardinal et al.[35] In their work, Cardinal et al.[35] created a map that shows the Peclet number (Pe) on the y-axis, where ($Pe = EH_o/D_o$) and the sedimentation number (N_s) on the x-axis, where ($N_s = U_o/E$). In these dimensionless numbers, (E) is the evaporation rate as given by the velocity of the free surface, (H_o) is the initial coating thickness, (D_o) is the Stokes-Einstein diffusion coefficient, and (U_o) is the sedimentation velocity. Figure 6 shows the model results as a drying regime map from Cardinal et al.[35] with information relevant to the current research added. For additional details on the model estimations and calculations, see Supporting Information (S3) available online.

The predictions from Figure 6 show that the smaller silica particles (Silica-M0.3) lie in the evaporation region and are predicted to accumulate at the free surface during drying. Meanwhile, the larger silica particles (Silica-M0.9) are predicted to sediment during drying, though the position on the map indicates the possibility of some accumulation from evaporation. For the 30 vol% Silica-M0.9 coating, sedimentation allows the coating to form a continuous

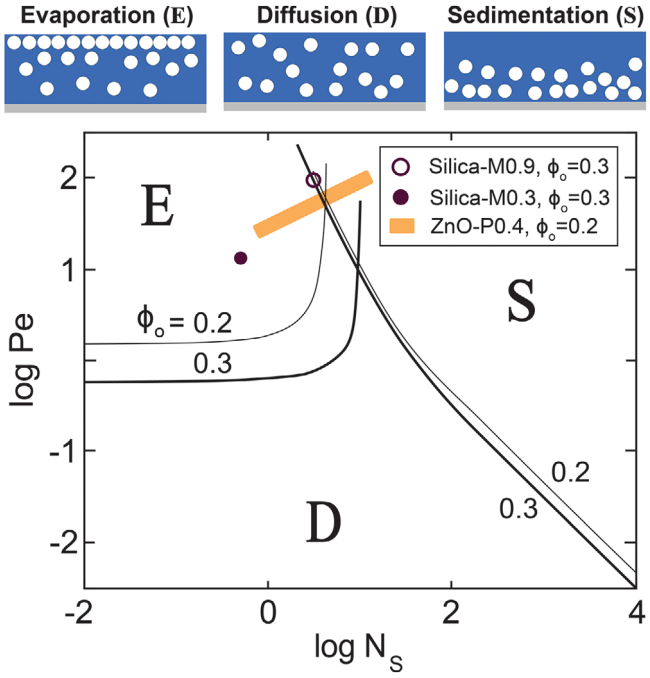

FIGURE 6 Top: Diagrams showing particle distributions through the thicknesses of coatings dominated by evaporation (E; particle accumulation at the free surface), diffusion (D; uniform particle concentration), and sedimentation (S; particle accumulation at the substrate). Bottom: Drying regime map from Cardinal et al.[35] with boundaries for distribution regions given two initial particle volume fractions (ϕ_0). Peclet number (*Pe*) and sedimentation number (N_s) were estimated to place the particle systems used in this research on the map.

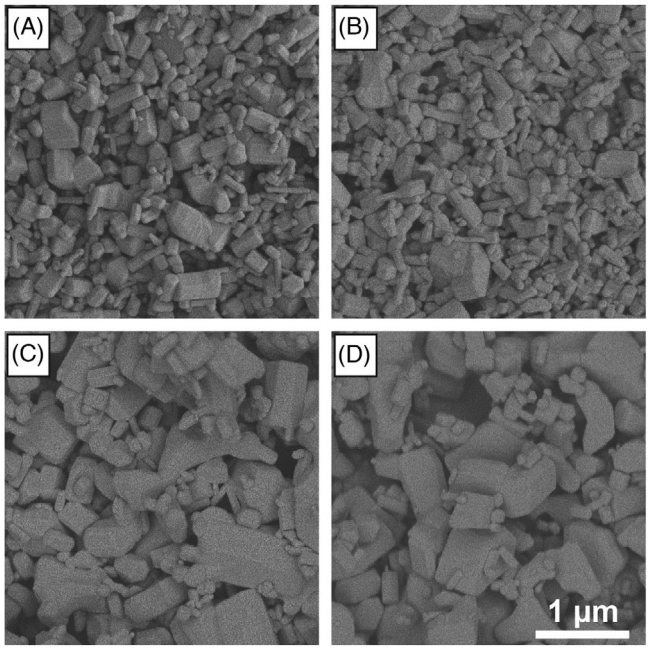

FIGURE 7 SEM Images of the (A) top and (C) bottom surface of a 46 ± 5 μm thick ZnOP0.4 coating, and the (B) top and (D) bottom surface of an 86 ± 7 μm thick ZnOP0.4 coating. The thinner coating (A) and (C), and thicker coating (B) and (D) show similar surface microstructure.

consolidated region adjacent to the substrate; this result is consistent with the Cryo-SEM study by Price and coworkers.[11] Such a coating is likely to remain uniformly saturated during drying. By contrast, in the 30 vol% Silica-M0.3 coatings, particles appear to accumulate at the free surface during drying, as evidenced by the opalescence in our images. Luo et al.,[34] documented such opalescence with the ordering of monodisperse particles accumulating on the free surface of a drying coating using Cryo-SEM. Therefore, in the Silica-M0.3 coatings, particles likely consolidate into a network on the surface, leaving pockets of unconsolidated suspension adjacent to the substrate in the thicker regions near the walls.[32] These inherent nonuniformities in saturation may lead to lateral drying.

An impractically low drying rate would be necessary to dry the Silica-M0.3 coatings outside of the evaporation region. Hence, an alternative particle system was selected. Since sedimentation is impacted by particle density, denser particles are more likely to dry in the sedimentation region with practical drying times. It is interesting that the work of Bauer et al.[10] is consistent with this expectation. They report uniform drying and stress development in coatings prepared from suspensions of zirconia particles, which are relatively dense compared with silica.

To improve saturation uniformity in coatings prepared from suspensions with smaller-sized particles, a denser material, zinc oxide ($\rho = 5.61$ g/cm^3, over twice the density of silica), was selected. The polydisperse zinc oxide powder used in this research is described in Table 1 (ZnO-P0.4). Although the model discussed above assumes monodisperse particles, we can predict the drying regime for different particle sizes of zinc oxide and use this prediction as a guide. Considering the particle size distribution, the drying regime for the 20 vol% ZnO-P0.4 system is plotted as a line in Figure 6, with the left end of the line representing the smallest particles and the right end the largest. The distribution is split between the sedimentation-dominated regime and the evaporation-dominated regime. Therefore, some particles may accumulate on the free surface and potentially disrupt drying uniformity. Nonetheless, the system is promising due to the tendency toward sedimentation.

To explore the role of polydispersity on microstructure, SEM images were taken of both the top (free surface) and bottom (substrate adjacent) surfaces of the ZnO-P0.4 coatings prepared at two different coating thicknesses (see Figure 7). The thinner, 46 ± 5 μm, and thicker, 86 ± 7 μm, coatings showed a higher concentration of large particles at the bottom surfaces and an abundance of small particles,

with some large particles interspersed, at the top surfaces. Thus, there was some stratification in these coatings during drying, consistent with that noted in other polydisperse systems.[12,35–37] Based on the SEM images, this stratification appears to be very similar for both the thin and thick coatings. Thus, stratification is not expected to impact comparisons of stress profiles between thin and thick coatings.

3.3 | Stress and fracture in zinc oxide particle coatings

To explore stress development in cracking coatings, a range of volume of the ZnO-P0.4 suspension was deposited on walled cantilevers to give dried coating thicknesses above and below the CCT. Coatings did not crack when the dried thicknesses were below ~53 μm, so this value was considered the CCT for this study. Fractures tended to begin at the wall where the coating was locally thicker; the dried coating was considered cracked if the cracks were visible during video imaging. No cracks were visible under an optical microscope (Hirox) in coatings with thicknesses below the CCT. Figure 8 shows stress development data and surface images from zinc oxide coatings with thicknesses below and above the CCT.

The stress profile for the thinner, crack-free coating has a similar character to the uniformly dried Silica-M0.9 suspensions in Figure 5. Likewise, Figure 8 images (1a)–(1e) shows no indication of lateral drying or cracking. As in the case of Silica-M0.9 (Figure 5), Figure 8 shows that the ZnO-P0.4 coating is stress-free early in drying (1a, 1b). The coating experiences a steep increase to a peak (1c), presumably due to the formation of liquid menisci within the compacted particle network, followed by a stress decline (1d) as water evaporates from the particle network. Once dried (1e), the ZnO-P0.4 coatings have a flat white appearance under room lighting conditions.

Figure 8 also shows the stress profile and surface images for a thicker coating. Like the thinner coating, the thicker coating is stress-free in the early stages of drying (2a) when the suspension is supersaturated. The thicker coating remains stress-free longer than the thinner coating, as expected. The stress then rises sharply to a peak stress (2b). Cracks appear just after the point of peak stress, becoming readily visible in Figure 8 image (2c). It is likely fracture begins with cracks too small to visualize with the camera; however, with our present imaging system, it is difficult to provide a more exact time point for fracture onset. As shown in images (2c)–(2e), many of the initial cracks in the dried coating are perpendicular to cantilever walls, and then, in some places, secondary cracks appear to connect

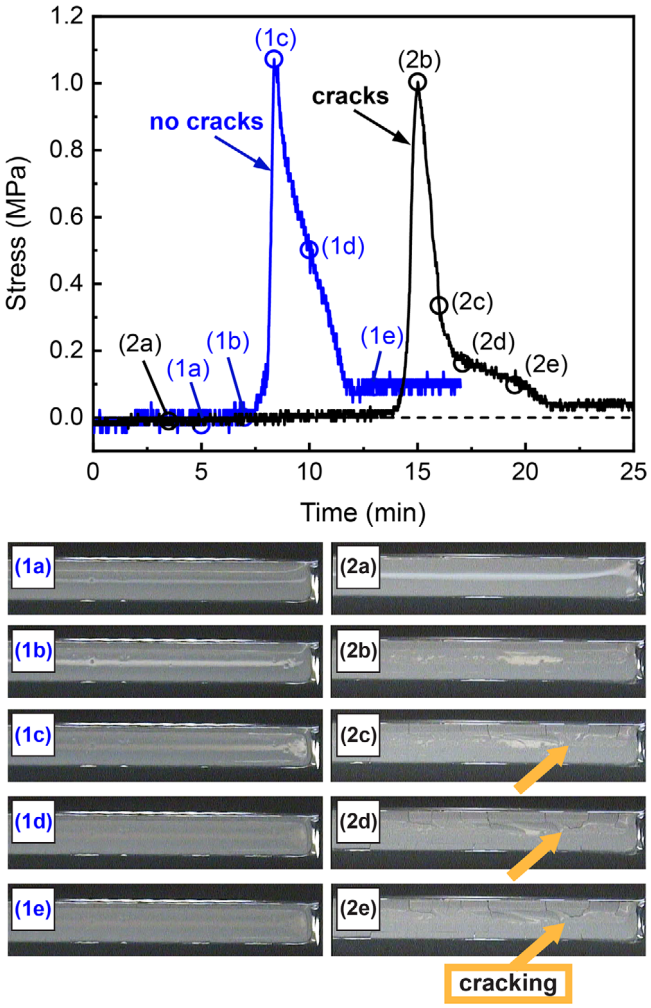

FIGURE 8 Stress development for coatings prepared from the ZnO-P0.4 suspension. Top: Stress measurement data for a thinner, crack-free coating (blue) with a thickness of 40 ± 8 μm and a thicker, cracked coating (black) with a thickness of 77 ± 10 μm. Bottom: Images of the coating surfaces taken in situ at the time points indicated. Data were collected at 22.1°C and 14% RH.

two or more of these cracks to form islands. This sort of cracking pattern is characteristic of mud cracking.[38,39]

After the peak, stress decreases with further drying at points (2c) and (2d), as shown in Figure 8. Unlike the crack-free coatings, the stress drop in the thicker, cracked coating has two stages: a rapid decrease ((2b), (2c)) followed by a slower decrease ((2c)–(2e)). After time (2d), the extent of fracture at the coating surface remains unchanged. However, localized curling of delaminated coating sections continues until (2e), after which the coating surface remains unchanged. It should also be noted that after cracks form, the coating is not a continuous solid, and hence, the conversion of the measured deflection to stress is no longer strictly valid. However, fractured sections that remain adhered to the substrate continue to contribute

to the deflection. Therefore, the calculated stress after cracking is a useful metric for comparison.

With uniform drying conditions in the ZnO-P0.4 coating, stress measurements showed the sequence of events associated with coating fracture during drying more clearly than the Silica-M0.3 coatings, which did not dry uniformly. Given that the first stage of the stress decline in Figure 8 ((2b), (2c)) coincides with the appearance of the cracks, we expect that this initial rapid decline is primarily due to cracking. The second intermediate stage ((2c), (2d)) appears to include a contribution from cracking as well as evaporation. The final slower stage of stress decrease ((2d), (2e)) is likely dominated by water loss from the particulate network due to evaporation, as it resembles the slower decline observed for crack-free coatings and visible changes to cracks do not occur in this period. This sequence aligns with other work in one-dimensional drying,[18] where cracking occurs just after the coating irreversibly aggregates into a solidnetwork, and cracks remain present throughout the emptying of the pore space.

In Figure 8, the peak stress for the thinner coating is similar in magnitude to the peak stress experienced by the thicker coating, yet it did not crack. This result is expected based on the following definition of the CCT: the thickness above which the extension of a crack is energetically favorable.[40,41] Lange et al.[40] used an energetic analysis to show that the rate of free energy reduction with crack extension is higher in thicker coatings and those under higher stress. Hence, for coatings experiencing the same stress, crack extension is more likely to be energetically favorable in the thicker coating.

To observe the relationship between stress and coating thickness, the ZnO-P0.4 suspension was deposited in varying volumes, and drying stress was measured for coatings ranging in average thickness from 38 to 97 μm. For crack-free coatings, the peak stress was found to be ~1.0 MPa as the average thickness varied from 38 to 53 μm, with no relationship between thickness and peak stress observed. Coatings between 53 and 74 μm would sometimes crack, whereas coatings greater than 74 μm consistently cracked. The unreliable fracture for coatings between 53 and 74 μm could be due to the variability of the coating thickness (see Supporting Information (S1) available online) as well as variability in flaw populations.

To better compare the stress profiles of cracking zinc oxide coatings with crack-free coatings, Figure 9 shows the data from Figure 8 (coatings (A) and (B)) replotted with data from additional cracking coatings (C–E), and the drying time was normalized to the time when the coating reached its peak stress (t_{max}). This scaling is analogous to that used by Tirumkudulu and Russel,[23] and accounts for

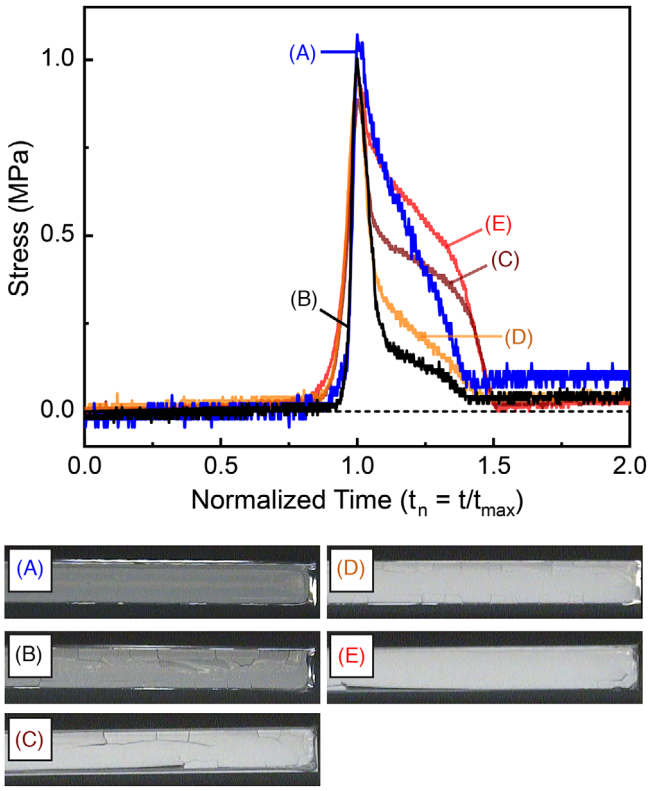

FIGURE 9 Top: Data from Figure 8 (coating (A) - crack free and coating (B) - cracked) along with three other ZnO-P0.4 cracking coatings (C)–(E) plotted as stress as a function of normalized time. The average thickness of coatings (C)–(E) were 93 ± 10 μm, 86 ± 7 μm, and 87 ± 5 μm, respectively. Data for (C)–(E) were collected at 22.2°C and 28% RH. Bottom: Images of the final dried coatings.

the effect of coating thickness and the drying rate associated with different relative humidities. Because the coatings dried uniformly, the time of peak stress occurs when the coating reaches equal saturation over the coating area and at an equal liquid volume fraction for all coating thicknesses. In Figure 9, both crack-free (A) and cracked coatings (B–E) reach a peak stress at normalized time ($t_n = 1$) as expected, and all profiles (A–E) reach stable, residual coating stress at approximately the same normalized time (t_n ~1.4).

All of the cracking coatings (B)–(E) in Figure 9 reached similar peak stresses. For cracking particulate coatings, it has been predicted that the critical stress for fracture decreases with increasing thickness.[24] However, there was insufficient data to quantitatively describe the relationship between peak stress and thickness in this work. Nonetheless, we observed that variations in the extent of fracture resulted in different stress profiles after the peak stress. Notably, coatings (D) and (E) had nominally the same average thickness at ~86 μm, yet the stress profiles (D) and (E) are noticeably distinct. Coating (D) experiences a large

drop in stress during fracture, like coating (B). However, coating (E) experienced a lesser drop in stress immediately after reaching its peak. As shown in the images of the dried coatings in Figure 9, coatings (B) and (D) have mud-like cracks perpendicular to the length of the cantilever, whereas coatings (C) and (E) both have larger cracks parallel to the length of the cantilever and delamination. Additionally, the coating (E) has fewer cracks, with only one large crack and delamination adjacent to the coating wall. It follows then that the nature of stress release is related to the extent of fracture. If the coating cracks to a greater extent, with longer crack lengths apparent once fully dried, the stress profile shows greater stress release just after the time of peak stress.

4 | CONCLUSION

This study demonstrates a method for studying coating stress and fracture with cantilever beam deflection. There were two keys to the development of the method. First, uniform drying (i.e., without in-plane saturation gradients) was encouraged using cantilever walls to prevent premature solidification at edges. Second, to achieve drying uniformity in coatings that also crack, the particle system was selected such that the particles were small enough for cracking to occur at a practical CCT and dense enough so particle accumulation at the free surface during drying was limited. In this work, zinc oxide with an average size of ~0.4 μm was selected, but many other ceramics could be studied, and it is possible to also decrease the drying rate to broaden the range of particle density. With this method, the stress profile features that correlate with cracking in particulate coatings were also identified. All coatings were stress-free during drying until the particle concentration reached compaction at which time the stress rose to a peak. After the peak stress, differences between crack-free and cracking coatings were apparent. The signature of a cracked coating is a two-stage stress decline after the peak: a steeper decline due to cracking and a slower decline due to the evaporation of water from the pore space and lessening of the capillary pressure effect. This signature can be useful to identify the formation of cracks during drying. Additionally, it was also possible to qualitatively determine the extent and nature of cracking by examining the stress release in time-normalized stress profiles. The method is therefore well-suited to studies aimed at assessing formulation or process changes designed to prevent cracking. Future developments of this method include improving the coating thickness uniformity by decreasing the contact line pinning on the walls and enhancing the in situ imaging technique. These improvements would allow for comparisons with theoretical predictions[13,24] and a better understanding of the onset of fracture.

ACKNOWLEDGEMENTS

The authors gratefully acknowledge support from the Coating Process Fundamentals Program of the Industrial Partnership for Research in Interfacial and Materials Engineering (IPRIME) at the University of Minnesota, thank Matt Hausladen, Prof. Michael Manno, Dr. Krystopher Jochem, Dr. Yuhai Xiang, and Olivia Dykes for their contributions to this project, and thank Dr. Yan Wu for her work leading up to this project. Parts of this work were carried out at the following facilities: (1) the Characterization Facility, the University of Minnesota (supported by MRSEC, award number DMR-2011401, and the NNCI, award number ECCS-2025124), and (2) the Minnesota Nano Center (supported by NNCI, award number ECCS-2025124).

ORCID

Annie Moorhead https://orcid.org/0009-0006-1106-7798
Lorraine F. Francis https://orcid.org/0000-0003-2516-2957

REFERENCES

1. Sørensen PA, Kiil S, Dam-Johansen K, Weinell CE. Anticorrosive coatings: a review. J Coat Technol Res. 2009;6(2):135–76.
2. Liu H, Wu YP, Rahm E, Holze R, Wu HQ. Cathode materials for lithium ion batteries prepared by sol-gel methods. J Solid State Electrochem. 2004;8(7):450–66.
3. Dimitriou E, Michailidis N. Printable conductive inks used for the fabrication of electronics: an overview. Nanotechnology. 2021;32(50):502009.
4. Kumano N, Kudo K, Suda A, Akimoto Y, Ishii M, Nakamura H. Controlling cracking formation in fuel cell catalyst layers. J Power Sources. 2019;419:219–28.
5. Rollag K, Juarez-Robles D, Du Z, Wood DL, Mukherjee PP. Drying temperature and capillarity-driven crack formation in aqueous processing of Li-ion battery electrodes. ACS Appl Energy Mater. 2019;2(6):4464–76.
6. Gokhale P, Mitra D, Sowade E, et al. Controlling the crack formation in inkjet-printed silver nanoparticle thin-films for high resolution patterning using intense pulsed light treatment. Nanotechnology. 2017;28(49):495301.
7. Jiang Z, Hsain Z, Pikul JH. Thick free-standing metallic inverse opals enabled by new insights into the fracture of drying particle films. Langmuir. 2020;36(26):7315–24.
8. Holmes DM, Vasant Kumar R, Clegg WJ. Cracking during lateral drying of alumina suspensions. J Am Ceram Soc. 2006;89(6):1908–13.
9. Chiu RC, Cima MJ. Drying of granular ceramic films: II, drying stress and saturation uniformity. J Am Ceram Soc. 1993;76(11):2769–77.
10. Bauer C, Cima M, Dellert A, Roosen A. Stress Development during drying of aqueous zirconia based tape casting slurries

measured by transparent substrate deflection method. J Am Ceram Soc. 2009;92(6):1178–85.
11. Price KK, Wu Y, McCormick AV, Francis LF. Stress development in hard particle coatings in the absence of lateral drying. J Am Ceram Soc. 2015;98(7):2214–22.
12. Wu Y, Francis LF. Effect of particle size distribution on stress development and microstructure of particulate coatings. J Coat Technol Res. 2017;14(2):455–65.
13. Yow HN, Goikoetxea M, Goehring L, Routh AF. Effect of film thickness and particle size on cracking stresses in drying latex films. J Colloid Interface Sci. 2010;352(2):542–48.
14. Payne JA, McCormick AV, Francis LF. In situ stress measurement apparatus for liquid applied coatings. Rev Sci Instrum. 1997;68(12):4564–68.
15. Deegan RD, Bakajin O, Dupont TF, Huber G, Nagel SR, Witten TA. Capillary flow as the cause of ring stains from dried liquid drops. Nature. 1997;389(6653):827–29.
16. Holmes DM, Tegeler F, Clegg WJ. Stresses and strains in colloidal films during lateral drying. J Eur Ceram Soc. 2008;28(7):1381–87.
17. Corcoran EM. Determining stresses in organic coatings using plate beam deflection. J Paint Technol. 1969;41(538):635–40.
18. Goehring L, Clegg WJ, Routh AF. Solidification and ordering during directional drying of a colloidal dispersion. Langmuir. 2010;26(12):9269–75.
19. Goehring L, Clegg WJ, Routh AF. Plasticity and fracture in drying colloidal films. Phys Rev Lett. 2013;110(2):024301.
20. Dufresne ER, Corwin EI, Greenblatt NA, et al. Flow and fracture in drying nanoparticle suspensions. Phys Rev Lett. 2003;91(22):224501.
21. Chiu RC, Garino TJ, Cima MJ. Drying of granular ceramic films. I. Effect of processing variables on cracking behavior. J Am Ceram Soc. 1993;76(9):2257–64.
22. Yamamura M. Adsorption-mediated nonlinearity of critical cracking thickness in drying nanoparticle–polymer suspensions. AIChE J. 2021;67(5):e17229.
23. Tirumkudulu MS, Russel WB. Cracking in drying latex films. Langmuir. 2005;21(11):4938–48.
24. Singh KB, Tirumkudulu MS. Cracking in drying colloidal films. Phys Rev Lett. 2007;98(21):218302.
25. Lee WP, Routh AF. Why do drying films crack? Langmuir. 2004;20(23):9885–88.
26. Wu Y. Drying and cracking behavior of aqueous particulate (Dissertation on the internet), Minneapolis, MN: University of Minnesota; 2018 [cited 2023 Jul 15]. Available from: http://conservancy.umn.edu/handle/11299/196512
27. Cesarano Iii J, Aksay IA, Bleier A. Stability of aqueous α-Al2O3 suspensions with Poly(methacrylic acid) Polyelectrolyte. J Am Ceram Soc. 1988, 71(4):250–55.
28. Holzman N, Francis LF. Pneumatic system design for direct write 3D printing. In: Bourell DL, Crawford RH, Seepersad CC, Beaman JJ, Fish S, editors. 28th Annual International Solid Freeform Fabrication Symposium: conference proceedings [Internet]; 2017 Aug 7–9; University of Texas at Austin. Austin, TX (US): University of Texas at Austin; 2017. p. 647–51. Available from: https://repositories.lib.utexas.edu/handle/2152/89870
29. Hopcroft MA, Nix WD, Kenny TW. What is the Young's modulus of silicon? J Microelectromechanical Syst. 2010;19(2):229–38.
30. Franks GV, Sesso ML, Lam M, Lu Y, Xu L. Elastic plastic fracture mechanics investigation of toughness of wet colloidal particulate materials: influence of saturation. J Colloid Interface Sci. 2021;581:627–34.
31. Payne JA. Stress evolution in solidifying coatings. (Dissertation), Minneapolis, MN (US): University of Minnesota; 1998.
32. Price KK, McCormick AV, Francis LF. CryoSEM investigation of latex coatings dried in walled substrates. Langmuir. 2012;28(28):10329–33.
33. Perera DY. Internal stress in latex coatings. J Coat Technol. 1984;56(716):111–18.
34. Luo H, Cardinal CM, Scriven LE, Francis LF. Ceramic nanoparticle/monodisperse latex coatings. Langmuir. 2008;24(10):5552–61.
35. Cardinal CM, Jung YD, Ahn KH, Francis LF. Drying regime maps for particulate coatings. AIChE J. 2010;56(11):2769–80.
36. Schulz M, Keddie JL. A critical and quantitative review of the stratification of particles during the drying of colloidal films. Soft Matter. 2018;14(30):6181–97.
37. Trueman RE, Lago Domingues E, Emmett SN, Murray MW, Keddie JL, Routh AF. Autostratification in drying colloidal dispersions: experimental investigations. Langmuir. 2012, 28(7):3420–28.
38. Goehring L. Evolving fracture patterns: columnar joints, mud cracks and polygonal terrain. Philos Trans A Math Phys Eng Sci. 2013, 371(2004):20120353.
39. Santanach Carreras E, Chabert F, Dunstan DE, Franks GV. Avoiding "mud" cracks during drying of thin films from aqueous colloidal suspensions. J Colloid Interface Sci. 2007, 313(1):160–68.
40. Lange FF. Chemical solution routes to single-crystal thin films. Science. 1996, 273(5277):903–9.
41. Lei H, Francis LF, Gerberich WW, Scriven LE. Modeling stress and failure in shrinking coatings. MRS Online Proc Libr Arch. 2000 [cited 2023 Jul 15]; 653(1051). Available from: https://doi.org/10.1557/PROC-653-Z10.5

SUPPORTING INFORMATION

Additional supporting information can be found online in the Supporting Information section at the end of this article.

How to cite this article: Moorhead A, Francis LF. Characterizing stress development and cracking of ceramic particulate coatings during drying. J Am Ceram Soc. 2024;107:2837–48. https://doi.org/10.1111/jace.19644